(Received 31 July 2025, Accepted 10 September 2025, Scheduled 4 November 2025)

# Stability and Homogeneity of Muscle Phantom for Radiation Exposure from 5G Signals

Nur F. A. Asmadi[1], Aduwati Sali[1,2,*], Nurul H. Abd Rahman[3], Suriati Paiman[4,5], and Muhammad Z. Mohyedin[1,*]

[1]*Institute for Mathematical Research (INSPEM), Universiti Putra Malaysia, Serdang 43400, Selangor, Malaysia*
[2]*WiPNET Research Centre, Department of Computer and Communication Systems Engineering Faculty of Engineering, Universiti Putra Malaysia (UPM), Serdang, Selangor, Malaysia*
[3]*Microwave Research Institute (MRI), Universiti Teknologi MARA, Shah Alam 40450, Selangor, Malaysia*
[4]*Physics Department, Faculty of Science, Universiti Putra Malaysia, Serdang 43400, Selangor, Malaysia*
[5]*Functional Nanotechnology Devices Laboratory (FNDL), Institute of Nanoscience and Nanotechnology Universiti Putra Malaysia, Serdang 434000, Selangor, Malaysia*

**ABSTRACT:** The increasing deployment of 5G wireless technologies has raised the need for accurate, tissue equivalent phantoms to explore electromagnetic (EM) wave interactions with human body organs. This paper investigates stability and homogeneity of a low-cost, easy-to-fabricate human muscle phantom exposed to radiation exposure from 5G signals at frequencies of 700 MHz, 2.4 GHz, 3.5 GHz, and 20 GHz. The phantom was formulated using agar, polyethylene powder, sodium chloride, xanthan gum, sodium dehydro-acetate, and deionized water. Its permittivity and conductivity were measured using a vector network analyzer (VNA) over a 45-day period under low (2–5°C) and room temperature (27°C) storage. The results showed that the phantom was most homogenous at 20 GHz with the standard deviation (SD) of 0.51033 and the relative standard deviation (RSD) of 1.67%. For conductivity, the phantom demonstrated good homogeneity. However, it did not align with the corresponding real human muscle conductivity. The most homogenous conductivity was observed at 2.4 GHz with the SD and RSD of 0.06194 and 2.31% respectively. In terms of stability, relative permittivity was most stable at 20 GHz under room temperature conditions, with a maximum deviation of 21%. Stability of conductivity performance, on the other hand, was best maintained at 2.4 GHz under room temperature, where the highest observed deviation was 53%. The findings highlight the potential of using low-cost materials to fabricate phantoms with stable electromagnetic properties suitable for wireless exposure studies, although further optimization is needed for accurate conductivity matching.

## 1. INTRODUCTION

The increasing presence of radio frequency electromagnetic radiation (RF-EMR) from various sources including radio-communication systems, mobile phones, microwave ovens, and wireless networks has contributed to a growing environmental pollution known as electromagnetic smog [1]. This electromagnetic pollution is classified as non-ionizing radiation (NIR) which lacks ionizing energy required to break chemical bonds. However, the introduction of fifth-generation (5G) wireless communication has raised significant health risk concern among the public and scientific community due to its higher frequency operation. The potential health impacts of electromagnetic fields (EMFs) vary depending on both the frequency and intensity of exposure [2, 3]. Although numerous studies have investigated these effects, the results remain inconsistent across various biological endpoints. For example, the BioInitiative Report concluded that there is sufficient evidence to suggest possible long-term health risks, including carcinogenicity, associated with prolonged EMF exposure [4]. In contrast, evidence regarding short-term health effects remains inconclusive, with studies yielding mixed or insufficient results [5, 6].

The International Commission on Non-Ionizing Radiation Protection (ICNIRP) provides internationally recognized guidelines for limiting human exposure to electromagnetic fields (EMFs). In 2020, ICNIRP updated its recommendations, replacing the earlier guidelines for the 100 kHz to 300 GHz frequency range outlined in ICNIRP (1998), as well as the 100 kHz to 10 MHz range previously covered in ICNIRP (2010) for low-frequency exposures [7]. Due to ongoing debate and limited understanding regarding the biological effects of EMFs on the human body, tissue-equivalent phantoms are widely employed in research as controlled and reproducible platforms for investigating EMF-tissue interactions without involving human subjects [8]. These phantoms are essential for evaluating the safety and performance of wireless communication devices by simulating human tissue responses to electromagnetic fields. There are four types of phantoms which are liquid, solid, semisolid, and 3D-printed phantoms [9–2]. Each type of phantom has its own advantages and disadvantages based on recipe and fabrication methods [13, 14]. Among them, semisolid phantom is the most commonly used due to its ease of preparation, cost-effectiveness, and

* Corresponding authors: Aduwati Sali (aduwati@upm.edu.my); Muhammad Zamir Mohyedin (zamirmohyedin@upm.edu.my).

**TABLE 1**. Ingredients and functional roles in the fabrication of the muscle phantom.

| Ingredient | Purpose | Amount |
|---|---|---|
| Deionized Water | Main component | 210 mL |
| Agar | Hold the phantom's shape | 10 g |
| Sodium dehydro-acetate | As a preservative | 0.125 g |
| Sodium Chloride | Modifying the conductivity value of the phantom | 2.05 g |
| Xanthan gum | As a thickener | 3.125 g |
| Polyethylene Powder | Modifying the permittivity value of the phantom | 14.5 g |

mechanical properties similar to human tissues since it has high water content [11]. These features make it particularly suitable for biomedical applications, including the assessment of pulmonary disorders such as cardiac pulmonary edema, a condition characterized by fluid accumulation in the lungs as a consequence of heart disease [15] .

The selection of appropriate ingredients is critical in developing tissue-equivalent phantoms that accurately replicate the physical and mechanical properties of real human tissues. Modifying ingredients and composition ratios can significantly influence the phantom's overall properties and performance. Previous research work has included toxic ingredients such as sodium azide and TX-151 in phantom fabrication to achieve desired properties [16–19]. However, due to safety concerns, researchers have progressively moved toward safer alternatives. In 2018, sodium dehydro-acetate was adopted as a substitute for sodium azide, while xanthan gum has replaced TX-151 in many formulations [11, 20, 21]. In this study, sodium dehydro-acetate and xanthan gum were employed because of their accessibility, cost-effectiveness, and compatibility with achieving the desired semisolid consistency required for EMF exposure assessments.

However, despite the critical role of phantoms in EMF studies, few studies have systematically evaluated their stability over time [22], particularly under 5G exposure conditions. Stability of electrical properties (relative permittivity and conductivity) is a critical factor as it ensures the reproducibility and reliability of experimental results over extended periods. Any changes in the phantom's physical, chemical, or electromagnetic properties over time may compromise the validity of exposure assessments. Therefore, comprehensive stability tests are necessary to confirm its suitability for repeated use in EMF research environment. This study aims to investigate the homogeneity and stability of the muscle-equivalent phantom over 45 days by evaluating its relative permittivity and conductivity.

## 2. METHODOLOGY

### 2.1. Synthesization Method

The formulation of the phantom comprised six key components: deionized water, agar, sodium dehydro-acetate, xanthan gum, sodium chloride (NaCl), and polyethylene powder. Among them, polyethylene powder and NaCl play critical roles in modifying the phantom's electromagnetic properties to closely resemble the human muscle tissue. Specifically, polyethylene powder was included to adjust the permittivity value, whereas NaCl was included to tailor electrical conductivity value of the phantom. The agar acts as a gelling agent while xanthan gum was utilized as a thickening agent. Sodium dehydro-acetate was used as a preservative while the deionized water acts as a main material [11]. Table 1 summarizes the composition and functional role of each ingredient in the phantom formulation.

### 2.2. Synthesization Procedure of Muscle Phantom

The synthesization procedure of the muscle phantom is illustrated in Fig. 1. Initially, the amount of deionized water, agar, sodium dehydro-acetate, sodium chloride, xanthan gum, and polyethylene powder were measured according to the quantities specified in Table 1. The deionized water and agar were first mixed in a heating pot. Subsequently, sodium dehydro-acetate and sodium chloride were added to the mixture with continuous stirring. After the solution was completely dissolved, the mixture was then heated at a temperature of approximately 143°C and maintained at this temperature for 2–3 minutes until bubbling was observed. The heater was then turned off, and the solution was transferred to a mixer. At this stage, xanthan gum and polyethylene powder were gradually introduced and thoroughly blended. The final mixture was then immediately poured into the closed containers with the height of 6 cm to ensure that the phantom has a thickness of 6 cm. The basis of the thickness follows the semi-infinite medium assumption of the open-ended coaxial probe method. Specifically, the phantom thickness was set to be larger than the effective sensing and penetration depth at the lowest frequency tested (700 MHz) so that the probe does not interact with the container, air, or table, and the measured reflection arises solely from the phantom. The container is then stored in the fridge for solidification.

In this paper, phantom samples were prepared by repeating the synthesization steps and subsequently divided into two storage groups: low temperature (2°C to 5°C) and ambient room temperature (approximately 27°C). The aim was to evaluate the effect of storage conditions on the electromagnetic properties of the phantoms, specifically relative permittivity and conductivity. The day after synthesization, the complex permittivity and conductivity of all samples were measured using a Dielectric Probe Kit, connected to Vector Network Analyzer (VNA) at frequencies of 700 MHz, 2.4 GHz, 3.5 GHz, and 20 GHz as shown in Fig. 2. The measured data from each group were averaged to obtain representative values for analysis. Following

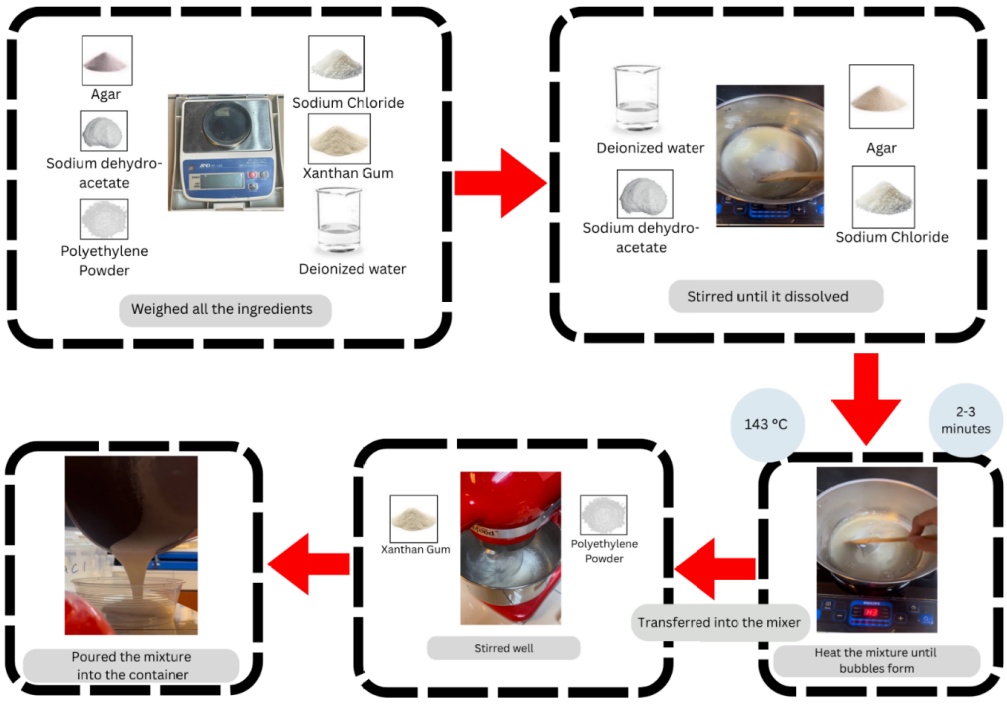


**FIGURE 1**. Procedures to synthesize muscle phantom.

initial measurements, the low-temperature group (LT) was returned to refrigerated storage, while the room-temperature (RT) group remained at ambient conditions. Measurements continued over a 45-day period to assess the stability of the phantom under both storage conditions.

45-day observation period was selected to reflect both immediate and extended usage scenarios of the phantom. In practical dosimetric or quality assurance (QA) delivery, a phantom fabricated in the laboratory may require several days for transportation to a testing facility, exposure experiments, and subsequent dielectric characterization. While such QA cycles are typically completed within a few days, evaluating stability over 45 days provides a conservative benchmark which ensuring that the phantom remains reliable even if fabrication, delivery, storage, or repeated testing is spread over several weeks. In addition, it is important to guarantee reproducibility and usability in different locations or repeated experiments.

### 2.3. Evaluation of Relative Permittivity Conductivity of the Phantom

The dielectric probe method relies on the reflection coefficient measured at the interface between the probe and the phantom. Using algorithms embedded in the VNA software, the complex permittivity, $\varepsilon^* = \varepsilon' - j\varepsilon''$, is extracted from the measured reflection data. The real part ($\varepsilon'$) corresponds to the relative permittivity of the material, while the imaginary part ($\varepsilon''$) accounts for dielectric losses. The conductivity ($\sigma$) can be obtained as follows:

$$\sigma = 2\pi f \varepsilon_0 \varepsilon''$$

where $f$ is the operating frequency, and $\varepsilon_0$ is the permittivity of free space $= 8.854 \times 10^{-12}$ F/m. This theoretical relationship provides the basis for converting VNA reflection measurements into the permittivity and conductivity values.

A dielectric probe connected to a VNA as displayed in Fig. 2(a) was applied to measure the relative permittivity ($\varepsilon'$) and conductivity ($\sigma$) of the muscle phantom. The probe test is considered as one of the most popular and easy to use techniques to measure electromagnetic properties. The probe is also nondestructive which does not affect measuring substrate. The probe has capability of measurement up to 20 GHz. Before starting the measurement, the probe was calibrated using 25 $cm^3$ of distilled water as illustrated in Fig. 2(b) as a reference to ensure the accuracy and reliability of the measurements.

To improve the contact between the probe and sample surface, outer edges of the phantom were carefully trimmed, as shown in Fig. 2(d), to eliminate any potential air gaps during measurement. The measurements were conducted at four key frequencies: 700 MHz, 2.4 GHz, 3.5 GHz, and 20 GHz. Measurements were taken from the surface of the phantom as shown in Fig. 3 at 14 different locations as indicated in Fig. 4. Each location was measured three times to improve consistency and minimize experimental error. The resulting data were then recorded for further analysis. The average values of the measured relative permittivity and conductivity were calculated. The complete experimental workflow is summarized in the flowchart presented in Fig. 5.

## 3. RESULTS AND DISCUSSIONS

Measurements of complex permittivity and conductivity were carried out using a Vector Network Analyzer (VNA) at four se-

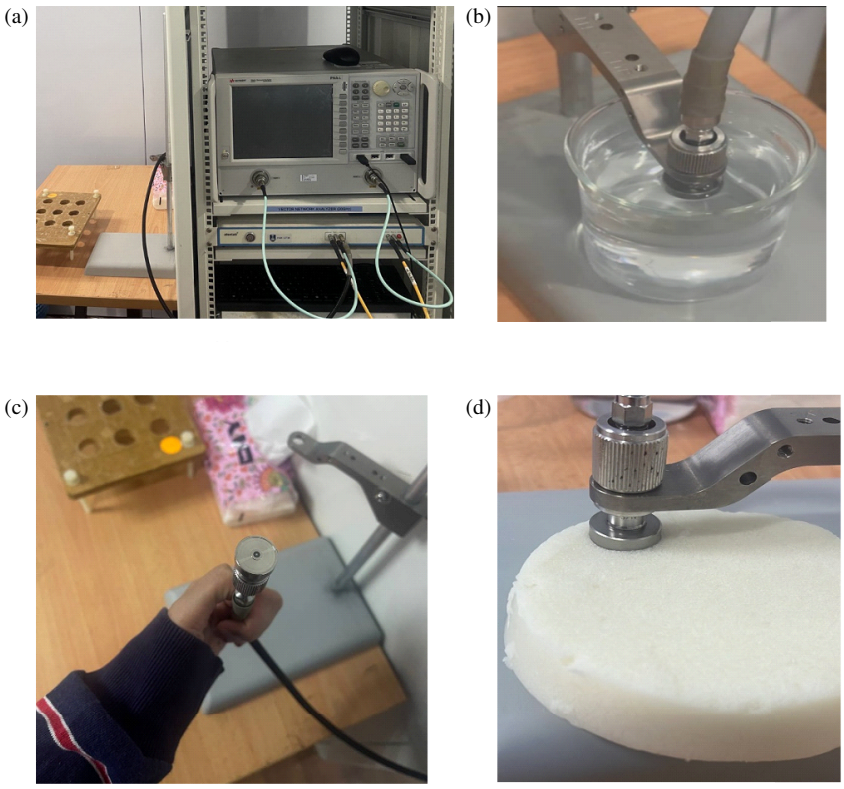

**FIGURE 2**. The measurement setup for the muscle phantom, (a) VNA and the measurable table, (b) calibration of VNA's dielectric probe with distilled water, (c) dielectric probe, (d) measurement process.

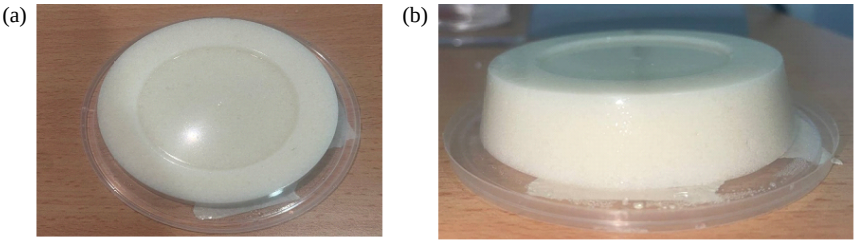

**FIGURE 3**. Surface of the phantom at (a) top view and (b) side view.

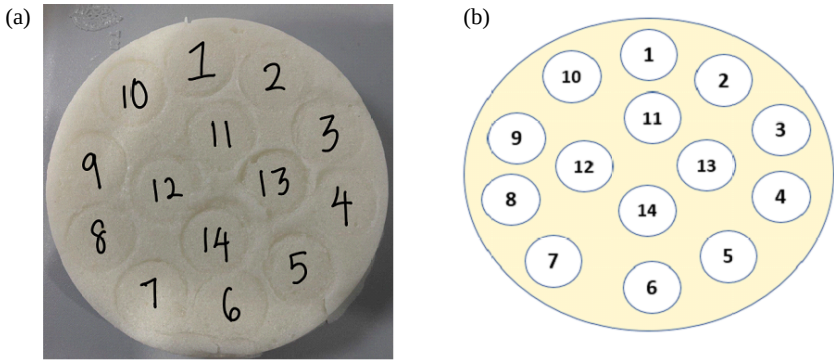


**FIGURE 4**. The locations of the probe after the measurement of complex permittivity on (a) fabricated muscle phantom, (b) diagram of locations of the probe.

lected frequencies: 700 MHz, 2.4 GHz, 3.5 GHz, and 20 GHz. The measurements were conducted under two storage conditions: low temperature (2°C–5°C) and room temperature (27°C). For each condition, data were collected three times at 14 different locations on the bottom surface of the fabricated phantom. The measured values were then averaged to obtain

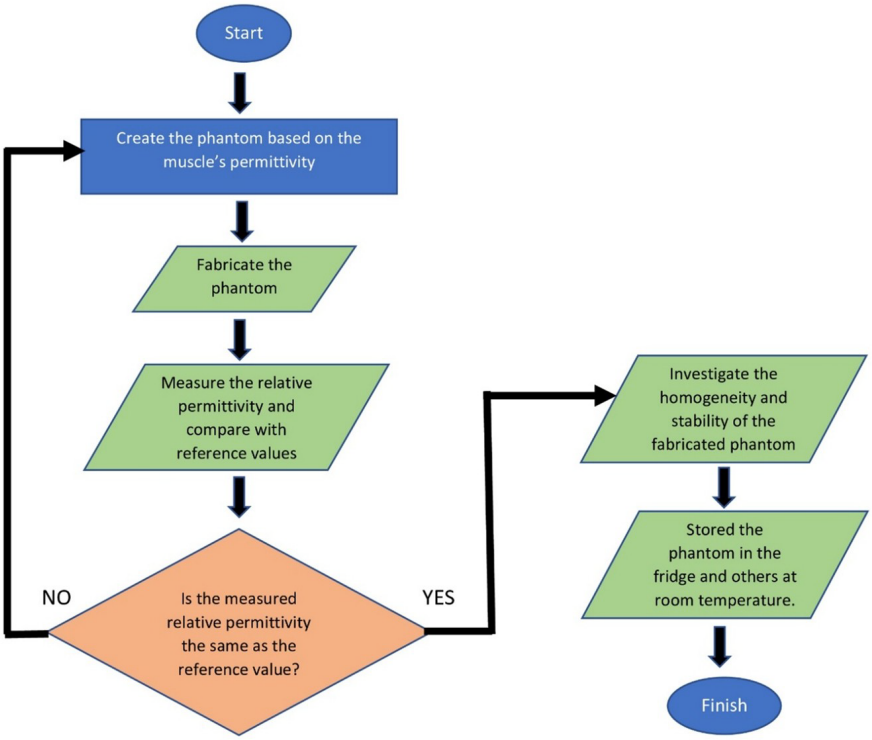


**FIGURE 5**. Flowchart of synthetization procedure.

**TABLE 2**. Summary of percentage deviations from the homogeneity analysis.

| Frequency | | 700 MHz | 2.4 GHz | 3.5 GHz | 20 GHz |
|---|---|---|---|---|---|
| **Relative Permittivity** | Standard Deviation (SD) | 0.8289 | 0.9115 | 0.8920 | 0.5103 |
| | Relative Standard Deviation (RSD) | 1.5270% | 1.7153% | 1.7464% | 1.6730% |
| **Conductivity** | Standard Deviation (SD) | 0.06401 | 0.06194 | 0.09734 | 0.98979 |
| | Relative Standard Deviation (RSD) | 3.0394% | 2.3123% | 2.8009% | 2.3506% |

overall values for both relative permittivity and conductivity. The results are divided into 2 parts: homogeneity and stability.

### 3.1. The Homogeneity Analysis of Synthesized Muscle Phantom

Figures 6(a)–(d) and 7(a)–(d) illustrate the averaged measured relative permittivity and conductivity at 14 different locations, respectively. The red horizontal line in each graph indicates the reference values for human muscle tissue. The standard accuracy from reference values is approximately 5% for relative permittivity and around 10% for conductivity as indicated by the error bars in the graph [8, 23]. As shown in Figs. 6(a)–(d), the measured relative permittivity across all frequencies and locations is closely aligned with the reference values with the maximum deviation of 7%, 4%, 5% and 6% for 700 MHz, 2.4 GHz, 3.5 GHz and 20 GHz, respectively.

In contrast, the measured conductivity presented in Figs. 7(a)–(d) shows consistently higher values than reference values of human muscle tissue. It is shown that, while the conductivity of the muscle phantom across all measured frequencies is homogeneous, the measured conductivity is deviate by 158% from the conductivity value of real human muscle. This deviation is likely attributed to the influence of sodium chloride, which significantly affects the phantom's conductivity. Therefore, it is recommended to reduce the sodium chloride content during synthesization to achieve better alignment with reference conductivity values [10].

Overall, the most homogeneous relative permittivity was observed at 20 GHz, where the standard deviation (SD) is 0.51033, and the relative standard deviation (RSD) is 1.67%. The most homogeneous conductivity was recorded at 2.4 GHz, with SD of 0.06194 and RSD of 2.31% as summarized in Table 2. Conversely, the lowest homogeneity for both relative permittivity and conductivity occurred at 700 MHz, with SD of 0.82892 and 2.10598 and corresponding RSD of 1.53% and 3.04% respectively, highlighting significant divergence from each other at this frequency. Nonetheless, the phantom still maintained homogeneity in relative permittivity and conductivity within 5% across all frequencies.

### 3.2. The Stability Analysis of Fabricated Muscle Phantom

Assessing the long-term stability of the muscle phantom is essential to ensuring its suitability for repeated use over extended periods. In this study, the stability of the phantom was moni-

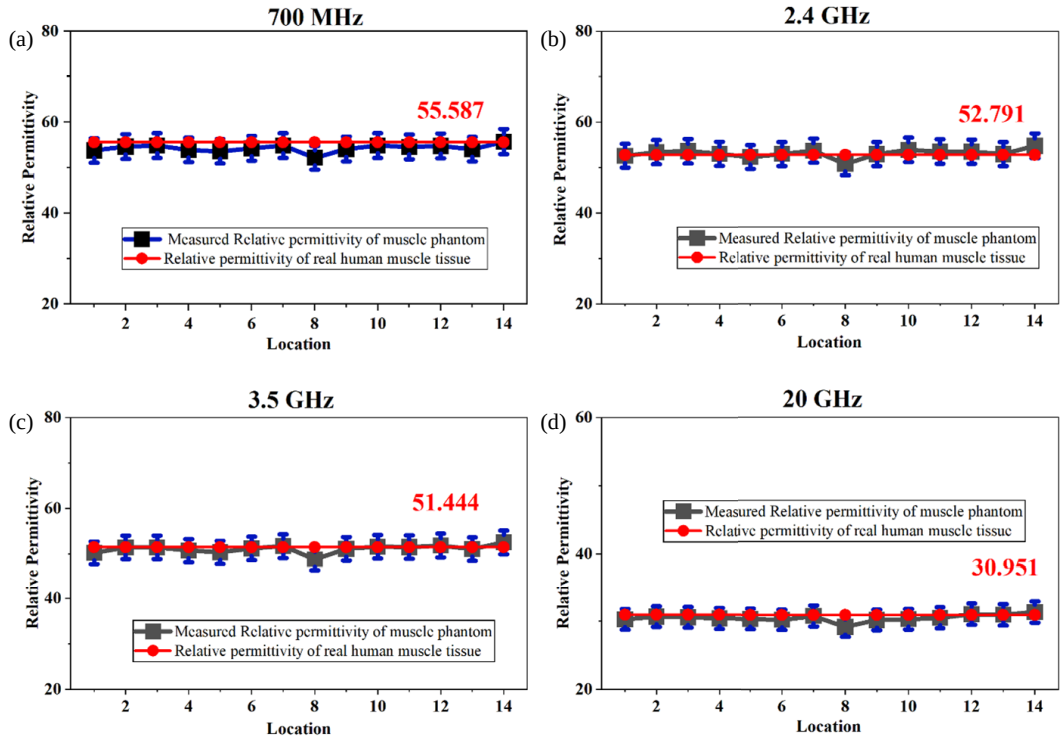


**FIGURE 6**. The homogeneity of measured relative permittivity with the frequency of (a) 700 MHz, (b) 2.4 GHz, (c) 3.5 GHz, (d) 20 GHz.

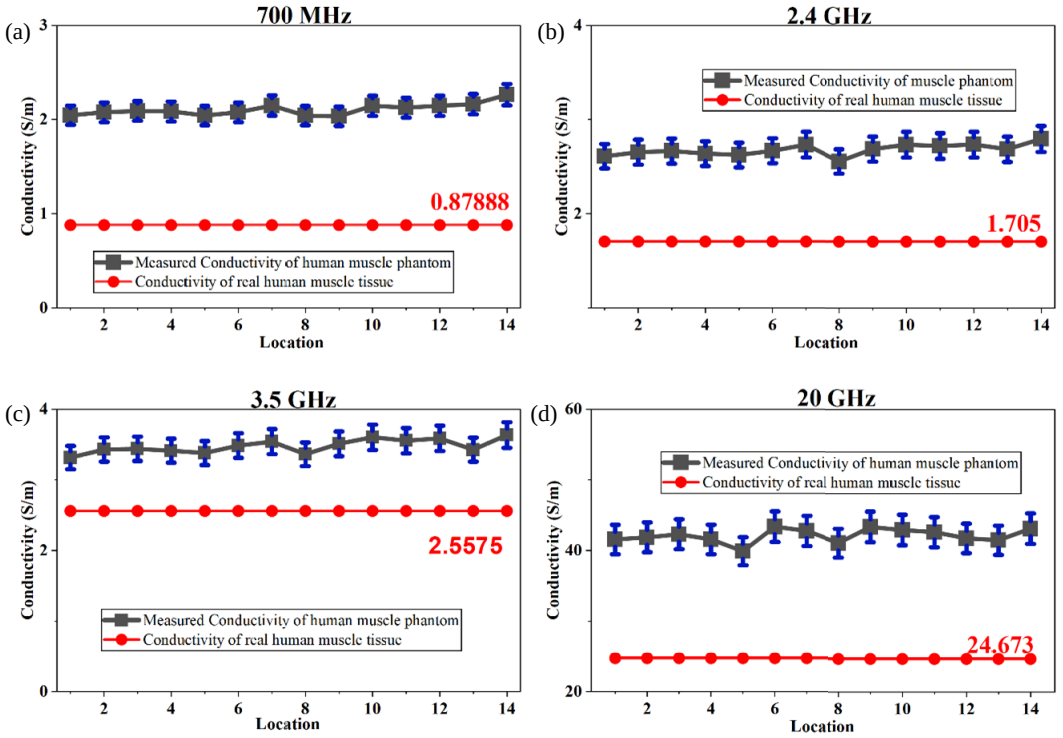


**FIGURE 7**. The homogeneity of measured conductivity with the frequency of (a) 700 MHz, (b) 2.4 GHz, (c) 3.5 GHz, (d) 20 GHz.

tored based on the relative permittivity and conductivity over a 45-day period under two storage conditions: low temperature (2°C–5°C) and room temperature (27°C). Figs. 8(a)–(d) and Figs. 9(a)–(d) illustrate the averaged relative permittivity and conductivity of the phantoms respectively over 45 days at four frequencies: 700 MHz, 2.4 GHz, 3.5 GHz, and 20 GHz throughout the study period. This evaluation was conducted to observe any temporal changes in the electromagnetic properties that could affect the phantom's performance.

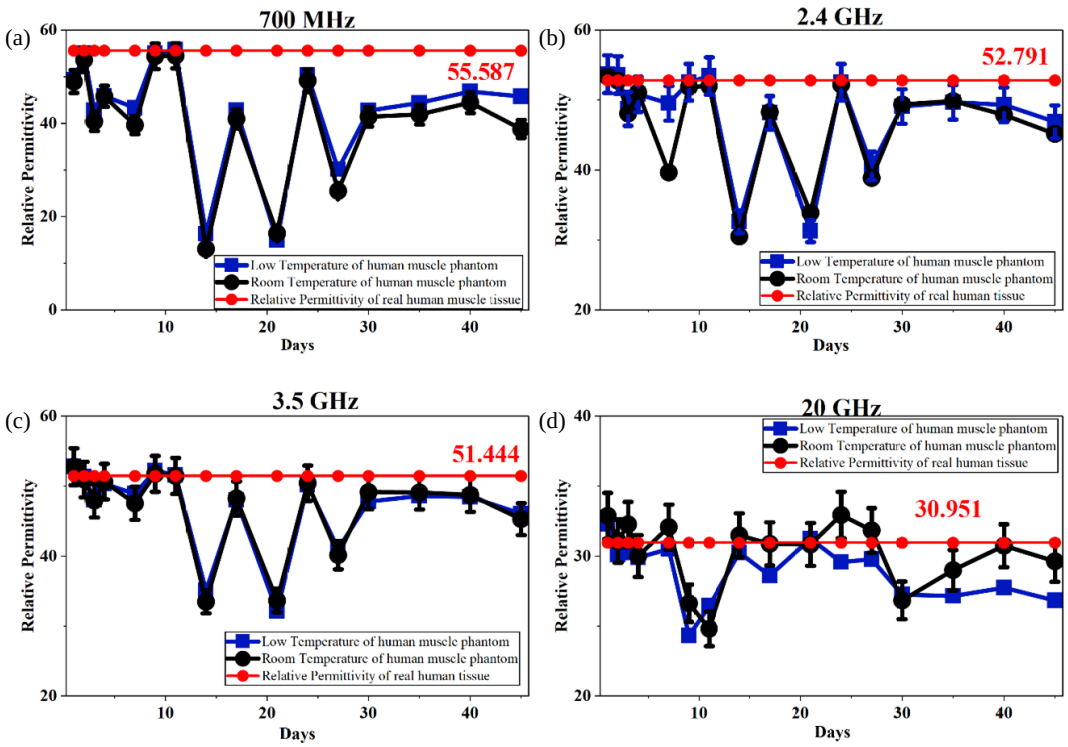


**FIGURE 8**. The stability of measured relative permittivity with the frequency of (a) 700 MHz, (b) 2.4 GHz, (c) 3.5 GHz, (d) 20 GHz at low temperature.

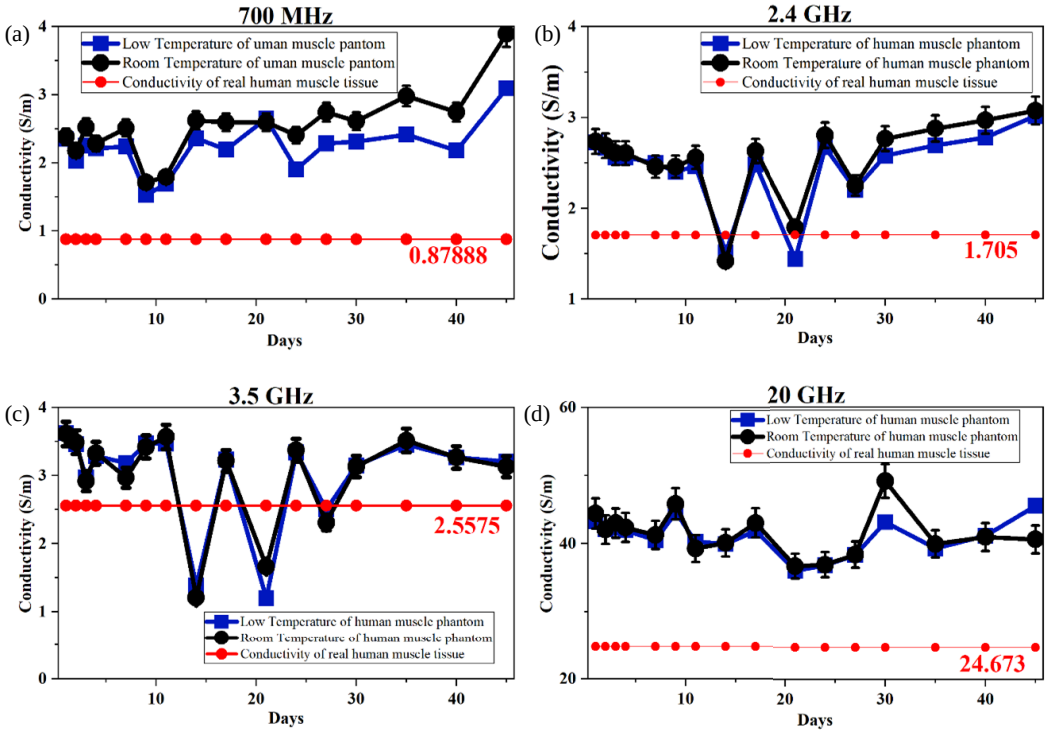


**FIGURE 9**. The stability of measured conductivity with the frequency of (a) 700 MHz, (b) 2.4 GHz, (c) 3.5 GHz, (d) 20 GHz.

As illustrated in Figs. 8(a)–(d), the averaged relative permittivity measurements at 700 MHz remained within ±5% of the reference values on days 2, 9, and 11 for both storage conditions, indicating completely stable behaviour during these periods. At 2.4 GHz, consistent and stable performance was observed on days 1, 2, 4, 9, 11, and 24 for both low and room temperature conditions. For 3.5 GHz, the phantom demonstrates stability on days 1, 2, 4, 7, 9, 11, and 24 under low temperature, and on days 1, 2, 3, 4, 7, 14, 21, 24, and 27 under room temperature conditions. At 20 GHz, stable relative permittivity values

were maintained on days 1, 2, 3, 4, 7, 14, 21, 24, and 27 at low temperature and on days 2, 3, 4, 7, 14, 17, 21, 27, 40, and 45 for room temperature conditions.

Regarding conductivity stability, as shown in Figs. 9(a)–(d), limited stability was observed at 2.4 GHz and 3.5 GHz, with each frequency exhibiting stability on only one day which is on day 21 for 2.4 GHz under room temperature and day 27 for 3.5 GHz under low temperature conditions.

Among all tested frequencies, 20 GHz under room temperature demonstrated the highest overall stability in relative permittivity. For conductivity, 2.4 GHz exhibited the most stable behaviour and also recorded the lowest maximum percentage deviation at 53%, indicating close alignment with the reference value. Again, 700 MHz exhibited the largest percentage deviations in both relative permittivity and conductivity stability, with deviations of 43% and 250%, respectively and both occurring under room temperature conditions.

It is important to consider how the observed deviations in dielectric properties may influence dosimetric outcomes when this phantom is employed in exposure studies. Specific absorption rate (SAR) is directly proportional to conductivity that can be expressed as:

$$\mathrm{SAR} = \frac{\sigma |E|^2}{2\rho}$$

where $E$ is the local electric field strength, and $\rho$ is the tissue density. The consistently higher conductivity values measured in the fabricated phantom would therefore lead to an overestimation of SAR in comparison to true biological tissue under identical exposure condition. For instance, at 3.5 GHz where conductivity deviation was most pronounced, SAR values derived using this phantom would be proportionally elevated, which may bias safety assessments if not corrected. Conversely, the close agreement in relative permittivity ensures that field distributions within the phantom remain representative of real muscle tissue, meaning that the phantom can reliably reproduce propagation and penetration depth characteristics of incident 5G signals. These findings highlight the importance of tuning sodium chloride content to better align conductivity with human tissue.

The instability of the phantom after several days can be explained by a few factors. First, although the phantom samples were stored in sealed container, gradual water loss could still occur during the measurement process when the containers were briefly opened. This evaporation reduces the effective permittivity as water has high dielectric constant. Besides that, agar and xanthan gum within the phantom typically undergo a structural relaxation phase after solidification. This can rearrange the chain of polymers which may influence the dielectric properties of the phantom. Finally, biological degradation was observed in the form of fungal growth on the phantom surface after extended storage. Such microbial activity may cause chemical breakdown of organic components which can alter the dielectric properties of the phantom. Collectively, these processes likely contributed to the deviation of the relative permittivity and conductivity of the phantom.

## 4. CONCLUSION

In conclusion, a semisolid muscle phantom was successfully synthesized, and its homogeneity and stability were evaluated at frequencies of 700 MHz, 2.4 GHz, 3.5 GHz, and 20 GHz under low temperature (2°C–5°C) and room temperature (27°C) conditions. The phantom was designed to replicate the electromagnetic properties of human muscle tissue using a formulation comprising agar, polyethylene powder, sodium chloride, xanthan gum, sodium dehydro-acetate, and deionized water. The measurements of electromagnetic properties of the phantom, including relative permittivity and conductivity, were performed using a Vector Network Analyzer (VNA), confirming the phantom's suitability for simulating real muscle tissue in relevant frequency ranges.

The results indicate that the synthesized phantom exhibits high homogeneity in relative permittivity at 20 GHz and in conductivity at 2.4 GHz. Regarding stability, the phantom showed the highest stability in relative permittivity at 20 GHz under room temperature conditions, while conductivity was most stable at 2.4 GHz, also under room temperature. For future work, modifications to the phantom composition especially reducing the amount of sodium chloride are recommended to achieve better alignment with reference conductivity values.

## ACKNOWLEDGEMENT

This work was funded by Universiti Putra Malaysia under the GP-IPS grant (No. 9815300). We also extend our appreciation to the Antenna Research Center (ARC), Faculty of Electrical Engineering, Universiti Teknologi MARA, Shah Alam, Selangor, Malaysia for providing the laboratory facilities and equipment essential to support this project.

## REFERENCES

[1] Butković, I., S. Vince, M. Lojkić, I. Folnožić, S. M. Tur, M. Vilić, K. Malarić, V. Berta, M. Samardžija, M. Kreszinger, and I. Z. Žaja, "Effects of 5G radiofrequency electromagnetic radiation on indicators of vitality and DNA integrity of in vitro exposed boar semen," *Theriogenology*, Vol. 230, 243–249, Dec. 2024.

[2] Ruijie, P., A. Sali, L. Li, M. Z. Mohyedin, and S. Qahtan, "Evaluation of personal radiation exposure from wireless signals in indoor and outdoor environments," *IEEE Access*, 2025.

[3] Tahir, I., A. Sali, S. Q. Wali, A. Ismail, D. Suka, and M. Z. Mohyedin, "Analysis of absorbed power density and power loss density in human skin model from 5G mmWave exposure," *Progress in Electromagnetics Research C*, Vol. 156, 93–100, 2025.

[4] Johansson, O., "Disturbance of the immune system by electromagnetic fields — A potentially underlying cause for cellular damage and tissue repair reduction which could lead to disease and impairment," *Pathophysiology*, Vol. 16, No. 2–3, 157–177, Aug. 2009.

[5] Bodewein, L., D. Dechent, D. Graefrath, T. Kraus, T. Krause, and S. Driessen, "Systematic review of the physiological and health-related effects of radiofrequency electromagnetic field exposure from wireless communication devices on children and adolescents in experimental and epidemiological human studies," *PLoS One*, Vol. 17, No. 6, e0268641, Jun. 2022.

[6] Calvente, I. and M. I. Núñez, "Is the sustainability of exposure to non-ionizing electromagnetic radiation possible?" *Medicina*

*Clínica (English Edition)*, Vol. 162, No. 8, 387–393, Apr. 2024.

[7] Ziegelberger, G., R. Croft, M. Feychting, A. C. Green, A. Hirata, G. D'Inzeo, K. Jokela, S. Loughran, C. Marino, S. Miller, *et al.*, "Guidelines for limiting exposure to electromagnetic fields (100 kHz to 300 GHz)," *Health Physics*, Vol. 118, No. 5, 483–524, 2020.

[8] Toyoda, S., T. Yamamoto, and K. Koshiji, "Prototype and evaluation of high-hydrous gel phantom for 100 kHz to 1 MHz using ATO/$TiO_2$," in *2021 43rd Annual International Conference of the IEEE Engineering in Medicine & Biology Society (EMBC)*, 6814–6817, Mexico, Nov. 2021.

[9] Sulaiman, N. H., N. A. Samsuri, M. K. A. Rahim, M. Inam, F. C. Seman, and N. Othman, "Phantom development for in vitro measurements of MICS band telemetry antenna," in *Journal of Physics: Conference Series*, Vol. 1502, No. 1, 012007, 2020.

[10] Ishido, R. and T. Onishi, "A study on the solid phantoms for 3–6 GHz and evaluation of SAR distributions based on the thermographic method," *IEICE Proceedings Series*, Vol. 11, No. 3B3-2, 577–580, 2004.

[11] Nizam, N. N. M., K. Kamardin, Y. Yamada, I. H. Idris, N. H. A. Rahman, and H. M. Kaidi, "Fabrication of human body phantom for body centric communication systems at 2.4 GHz," *International Journal of Integrated Engineering*, Vol. 12, No. 6, 20–26, 2020.

[12] Särestöniemi, M., D. Singh, R. Dessai, C. Heredia, S. Myllymäki, and T. Myllylä, "Realistic 3D phantoms for validation of microwave sensing in health monitoring applications," *Sensors*, Vol. 24, No. 6, 1975, Mar. 2024.

[13] Mobashsher, A. T. and A. M. Abbosh, "Artificial human phantoms: Human proxy in testing microwave apparatuses that have electromagnetic interaction with the human body," *IEEE Microwave Magazine*, Vol. 16, No. 6, 42–62, Jul. 2015.

[14] Guido, K., C. Matos, J. Ramsey, and A. Kiourti, "Tissue-emulating phantoms for in vitro experimentation at radio frequencies: Exploring characteristics, fabrication, and testing methods," *IEEE Antennas and Propagation Magazine*, Vol. 63, No. 6, 29–39, Dec. 2021.

[15] Irfana, P. P., R. S. Anand, A. Aprem, V. P. Vishal, S. Upendran, and S. Harikrisnan, "An economical method for modeling, fabrication, testing, and characterization of a bio-phantom for pulmonary edema," in *2023 IEEE International Conference on Recent Advances in Systems Science and Engineering (RASSE)*, 1–8, Kerala, India, Nov. 2023.

[16] Ito, K., K. Furuya, Y. Okano, and L. Hamada, "Development and characteristics of a biological tissue-equivalent phantom for microwaves," *Electronics and Communications in Japan (Part I: Communications)*, Vol. 84, No. 4, 67–77, Apr. 2001.

[17] Chahat, N., M. Zhadobov, and R. Sauleau, "Broadband tissue-equivalent phantom for BAN applications at millimeter waves," *IEEE Transactions on Microwave Theory and Techniques*, Vol. 60, No. 7, 2259–2266, Jul. 2012.

[18] Chahat, N., M. Zhadobov, S. Alekseev, and R. Sauleau, "Human skin-equivalent phantom for on-body antenna measurements in 60 GHz band," *Electronics Letters*, Vol. 48, No. 2, 67–68, Jan. 2012.

[19] Mendes, C. and C. Peixeiro, "A dual-mode single-band wearable microstrip antenna for body area networks," *IEEE Antennas and Wireless Propagation Letters*, Vol. 16, 3055–3058, 2017.

[20] Islam, M. T., M. Samsuzzaman, S. Kibria, and M. T. Islam, "Experimental breast phantoms for estimation of breast tumor using microwave imaging systems," *IEEE Access*, Vol. 6, 78 587–78 597, 2018.

[21] Abd Rahman, N. H., Y. Yamada, and M. S. A. Nordin, "Analysis on the effects of the human body on the performance of electro-textile antennas for wearable monitoring and tracking application," *Materials*, Vol. 12, No. 10, 1636, May 2019.

[22] Kranold, L., J. Boparai, L. Fortaleza, and M. Popovic, "A comparative study of skin phantoms for microwave applications," in *2020 42nd Annual International Conference of the IEEE Engineering in Medicine & Biology Society (EMBC)*, 4462–4465, Montreal, QC, Canada, Jul. 2020.

[23] Fukunaga, K., S. Watanabe, and Y. Yamanaka, "Dielectric properties of tissue-equivalent liquids and their effects on specific absorption rate," *IEEE Transactions on Electromagnetic Compatibility*, Vol. 46, No. 1, 126–129, Feb. 2004.